Supporting Information

Pantazis et al. 10.1073/pnas.1004748107

SI Text

SI Materials and Methods. ***Second harmonic generating (SHG) signal profile analysis.*** SHG signal profiles of SHG nanocrystals ($n \geq 5$ for each nonlinear material) covering the spectral range from 380 to 720 nm were recorded using the META detector of the Zeiss LSM 510NLO microscope setup by tuning the wavelength from 780 to 970 nm. The background measured in a random region of the gel without SHG nanocrystals was subtracted. To make the results insensitive to changes in laser power or pulse width, the data have been corrected according to the following equation that is derived from the nonlinear nature of SHG:

$$\mathrm{SHG}_{\mathrm{Signal}} \propto (P_m)^2 \frac{T}{\tau},$$

where P_m is the mean laser power after the microscope objective for each wavelength, τ is the previously measured pulse width (1), and T is the pulse repetition rate (80 MHz). Obtained SHG signal values were normalized by setting the highest signal value to 100.

Control experiments of $BaTiO_3$ nanoparticle characterization. For SHG nanoparticle characterization (blinking property comparison and signal saturation comparison), we controlled several conditions to study presumably individual nanocrystals. First, the sample was ultrasonicated and nanofiltered. The presence of isolated nanocrystals was confirmed (see Fig. S2*A*) using atomic force microscopy in the tapping mode (AFM, Digital Instruments). A 2 μL drop of sample was applied to the surface of freshly cleaved mica and immediately analyzed. Second, SHG solutions were immobilized in 20% polyacrylamide gel to avoid clustering after nanofiltering. In addition, the weakest SHG signal intensities of $BaTiO_3$ were chosen for comparison to quantum dots (QDs) from "flatfielded" images, where spatial aberrations in illumination and viewing optics, and in detector sensitivity, were corrected as previously described (2) to rule out systematic deviations in sensitivity over the spatial field of view. Briefly, corrections were performed by the use of three "flatfield" images gathered in the absence of nanocrystals using comparable excitation and detection settings. One image was taken with the light path closed (detection noise only), whereas the other two were scans of low and high concentrations (125 μg/mL and 675 μg/mL) of 10,000 MW Dextran-Cascade blue (Invitrogen Corp.). Acquired data were used to insure that illumination and detector settings were such that observations were in the linear range of the SHG nanoparticle detection and characterization (see Fig. S2*B*).

Once we determined that we were imaging SHG nanocrystals in a linear range, a custom Matlab script was used to segment the SHG signal from gel-immobilized nanocrystal. After background subtraction, we integrated the SHG signal in the segmented areas corresponding to a single diffraction-limited spot. As previously described (3), the experimental distribution $\rho(I)$ of the SHG intensities I (counts/pixel) was fitted by a sum of Gaussians:

$$\rho(I) = \sum_{i=1}^{2} A_i \exp\left(-\frac{(I-\mu_i)^2}{2\sigma_i^2}\right),$$

where μ is the mean, σ_i is the standard deviation, and A_i the amplitude. We chose to fit the distribution to two Gaussians by eye. The experimental data indicated very good agreement with the theoretical sum of Gaussians ($R^2 = 0.89$, see Fig. S2*C*). Given the AFM data, the first and major peak suggests the presence of single $BaTiO_3$ nanocrystals.

In Vivo $BaTiO_3$ Nanocrystal Injection and Imaging. Up to 50 fmol of ultrasonicated and nanofiltered $BaTiO_3$ nanocrystals were injected as previously described (4). For ubiquitous SHG signal presence, $BaTiO_3$ nanocrystals were injected into the yolk of either zygote/one-cell stage wild-type embryos (see Fig. 4) or mutant embryos of the cls line (5), which has fewer iridophores (see Fig. S4 *A* and *B* and Movie S3). Embryos were raised at 28 °C in 30% Danieau solution (4). The injected embryos developed indistinguishably from uninjected counterparts ($n = 600$). Prior to SHG imaging, zebrafish were anesthetized with 0.015% tricaine methanesulfonate in 30% Danieau solution. Cell membranes were dyed with the vital counterstain BODIPY TR methyl ester (Invitrogen Corp.). Specimens were oriented in 1% agarose molds as previously described (6). Live images of SHG injected zebrafish were obtained with an LD C-APO 40×/1.1 objective on a Zeiss 510NLO microscope setup. For three-channel confocal image acquisition, a femtosecond pulsed laser tuned to 820 nm (for imaging endogenous SHG as well as for $BaTiO_3$ nanocrystals) and the 543 nm He/Ne laser line (for imaging BODIPY TR methyl ester) were used sequentially. Endogenous SHG detection was performed in transdirection using a HQ405/40M emission filter (Chroma Technology Corp.). $BaTiO_3$ nanocrystals detection was performed in both transdirection (see above) as well as in epidirection using a BP390-465IR emission filter. A mode-locked infrared laser line at 820 nm from a Ti::Sapphire laser (Coherent, Inc.) with an average laser power of at least 5 mW after the objective (for single $BaTiO_3$ nanocrystals in tissue) and at least 50 mW after the objective (for endogenous SHG) was used, respectively. Nanocrystals of this size—comparable to the size range of water-soluble QDs—often formed clusters over time requiring lower intensities.

$BaTiO_3$ nanocrystal imaging in mammalian tail tendon. Collagen, the main fibrous component of tendon, cartilage, skin, etc., has been previously shown to display a high SHG efficiency (7). In addition to imaging $BaTiO_3$ nanocrystals within zebrafish muscle tissue, where arrays of myosin provide endogenous SHG contrast, we compared achievable SHG signal intensities of $BaTiO_3$ nanocrystals to collagen within a mouse tail tendon, a tissue with large collagen deposits of high regularity. Ultrasonicated and nanofiltered $BaTiO_3$ nanoparticles were injected in mouse tail slices of 2–3 mm thickness. The injected tissue slices were oriented in 1% agarose. Images of SHG injected mouse tail tendon were obtained with an long-distance correction ring apochromat objective (LD C-APO) 40 x/1.1 objective on a Zeiss 510NLO microscope setup. A femtosecond pulsed laser tuned to 850 nm for imaging endogenous SHG as well as for $BaTiO_3$ nanocrystals was used. SHG signal detection was performed in this case in epidirection. Due to multiple tissue scattering and the fact that the wavelength range we employ for exciting and collecting SHG is in the Rayleigh scattering regime, initially forward-directed endogenous SHG from collagen is rerouted into the backward direction. This approach of endogenous SHG imaging comes with its limitations: (*i*) significant SHG signal reduction, because backscattered signal represents only a small fraction of total endogenous SHG, (*ii*) loss of SHG coherence when the SHG photon's travel distance before scattering (the scattering length) is smaller than the active SHG volume dimensions, and (*iii*) high levels of absorption of SHG photons due to the fact that SHG photons must travel a long average pathlength due to multiple tissue backscattering events before reaching the detector. However, SHG nanoprobe imaging does not rely on backscattering with its

above-mentioned limitations for endogenous SHG. On the contrary, the number of detectable photons is effectively increased because a fraction of the multidirectional SHG signal of $BaTiO_3$ is now rerouted into the backward direction.

Long-term photostability of $BaTiO_3$/Dextran-Alexa546 in vivo. For SHG/Alexa546 signal presence in a subpopulation of cells, single cell coinjections of $BaTiO_3$ nanoparticles and 10,000 MW Dextran-Alexa546 (Invitrogen Corp.) were performed at the 32-cell stage and imaged at the dome stage of zebrafish embryos. Specimens were oriented in 1% agarose molds as previously described (6). Live images of SHG injected zebrafish embryos were obtained with a LD C-APO 40 x/1.1 objective on a Zeiss 510NLO microscope setup. For two-channel confocal image acquisition, a femtosecond pulsed laser tuned to 820 nm (for imaging SHG nanocrystals) and the 543 nm He/Ne laser line (for imaging coinjected Dextran-Alexa546) were used sequentially. Note that nanocrystals present in cells form to some extent clusters over time due to anomalous subdiffusion (8), commonly observed also for other particles of this size range like water-soluble QDs.

Immunostaining Dechorionated 24 hpf zebrafish embryos were fixed using 4% paraformaldehyde (PFA) in PBS for 2 h at room temperature. After a brief wash with PBS, the PFA-fixed zebrafish embryos were embedded in 4% agarose, sectioned using the Vibratome Series 1000 (The Vibratome Co.). The specimens were subsequently permeabilized in PBST (PBS with 0.1% Triton X100) for 1 h. The tissue was then blocked in PBSTB (PBST with 0.5% BSA) overnight at 4 ºC. After blocking, the samples were incubated with primary antibodies diluted in PBSTB for 2 h at room temperature. Immunostainings were performed using mouse anti-Dystrophin (MANDRA1, 7A10, Hybridoma Bank) at a dilution of 1:500. Unbound primary antibody was removed by three washes with PBST. Subsequently, specimens were incubated with the secondary antibody diluted in PBSTB for 2 h. Immunostainings were performed with 90-nm $BaTiO_3$ nanocrystals, which were functionalized as previously described (9, 10) and conjugated to Cy5-coupled donkey anti-mouse IgG antibodies (Jackson ImmunoResearch Laboratories, Inc.) based on cross-linking reactions between amine groups on the $BaTiO_3$ nanocrystals and sulfhydryl groups on the IgG antibody (11). Unconjugated antibodies were removed by centrifugation and the final solution was used after nanofiltering to remove clustered conjugates at a dilution of 1:10. This step was followed by washes with PBST. Cell boundaries were visualized by counterstaining the tissue with fluorescent phalloidin-Alexa546 (Invitrogen Corp.). Images were acquired using a Zeiss 510NLO microscope. For three-channel confocal image acquisition, a femtosecond pulsed laser tuned to 820 nm (for imaging SHG), a 543-nm He/Ne laser line (for imaging phalloidin-Alexa546), and a 633 nm He/Ne laser line (for imaging Cy5) were used sequentially. Images were processed using Adobe Photoshop CS3 (Adobe Systems).

1. Dickinson ME, Simbuerger E, Zimmermann B, Waters CW, Fraser SE (2003) Multiphoton excitation spectra in biological samples. *J Biomed Opt* 8(3):329–338.
2. Stollberg J, Fraser SE (1988) Acetylcholine receptors and concanavalin A-binding sites on cultured Xenopus muscle cells: Electrophoresis, diffusion, and aggregation. *J Cell Biol* 107(4):1397–1408.
3. Kicheva A, et al. (2007) Kinetics of morphogen gradient formation. *Science* 315(5811): 521–525.
4. Westerfield M (1995) *The Zebrafish Book* (Univ of Oregon Press, Eugene, OR), 3rd Ed, pp 1–385.
5. Kelsh RN, et al. (1996) Zebrafish pigmentation mutations and the processes of neural crest development. *Development* 123:369–389.
6. Megason SG, Fraser SE (2003) Digitizing life at the level of the cell: High-performance laser-scanning microscopy and image analysis for in toto imaging of development. *Mech Develop* 120(11):1407–1420.
7. Roth S, Freund I (1979) Second harmonic generation in collagen. *J Chem Phys* 70:1637–1643.
8. Weiss M, Elsner M, Kartberg F, Nilsson T (2004) Anomalous subdiffusion is a measure for cytoplasmic crowding in living cells. *Biophys J* 87(5):3518–3524.
9. Hsieh CL, Grange R, Pu Y, Psaltis D (2009) Three-dimensional harmonic holographic microcopy using nanoparticles as probes for cell imaging. *Opt Express* 17(4): 2880–2891.
10. Kim P, et al. (2007) Phosphonic acid-modified barium titanate polymer nanocomposites with high permittivity and dielectric strength. *Adv Mater* 19 (7):1001–1005.
11. Xing Y, et al. (2007) Bioconjugated quantum dots for multiplexed and quantitative immunohistochemistry. *Nat Protoc* 2(5):1152–1165.

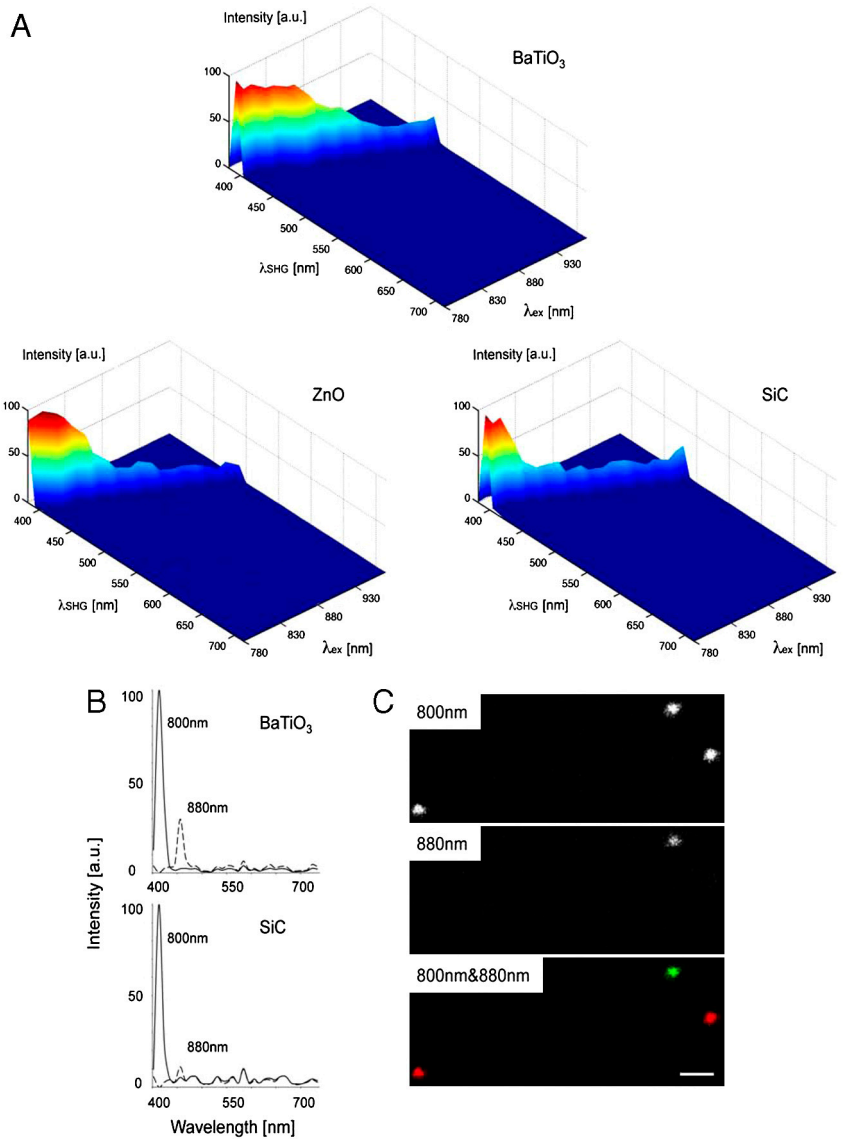

Fig. S1. SHG signal properties of $BaTiO_3$, ZnO, and SiC and multi-SHG imaging modality. (*A*) Displayed are the 3D normalized SHG signal data profiles of barium titanate ($BaTiO_3$), zinc oxide (ZnO), and silicon carbide (SiC) nanocrystals (signal ranging from 380 to 720 nm) generated by conventional two-photon excitation (excitation ranging from 760 to 970 nm). Note that the SHG signal peaks are always half the wavelength of the incident excitation wavelength. Regarding the higher frequency conversion efficiency at shorter wavelengths, this increase might be due to the fact that although the fundamental excitation frequency is far off resonance for the materials tested in our wavelength dependence experiment, the resulting second harmonic frequency is indeed close to resonance for all of the materials having band gap energies of around/less than 3 eV. Color code: dark blue corresponds to zero intensity and dark red corresponds to maximal intensity. (*B* and *C*) Multi-SHG imaging modality. (*B*) Displayed are the normalized SHG signal spectra of $BaTiO_3$ (*Upper*) and SiC (*Lower*) nanocrystals generated by tuning the excitation wavelength to 800 nm (solid line) and 880 nm (dashed line). (*C*) Single confocal sections showing comparable SHG signal intensities of immobilized $BaTiO_3$ and SiC nanocrystals in parallel. The noncentrosymmetric nanomaterials were sequentially excited with 800 nm (*Top*) and 880 nm (*Middle*), respectively. Whereas the SHG signal of SiC nanocrystals is only readily detectable at 800 nm, the SHG signal of $BaTiO_3$ nanocrystal is visible at both excitation wavelengths. In a multi-SHG imaging modality, relative intensities are sufficient to be compared in order to distinguish different SHG nanoprobe materials. Applying this information, one can now distinguish both nanomaterials (*Bottom*, false-colored picture: SiC nanocrystals in red, $BaTiO_3$ nanocrystal in green). Bar corresponds to 500 nm.

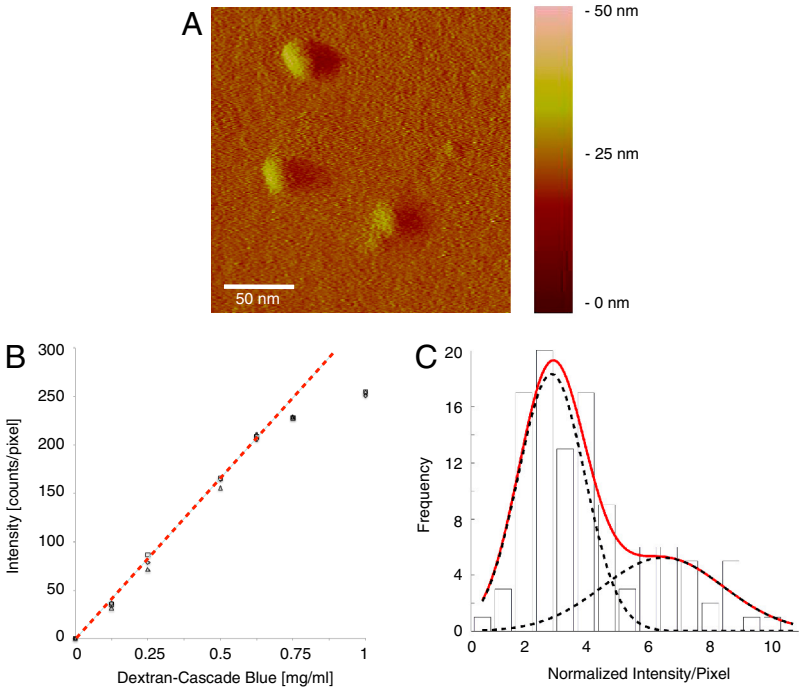

Fig. S2. Control experiments of $BaTiO_3$ nanocrystal characterization. (*A*) AFM image of individual, well-isolated $BaTiO_3$ nanocrystals. Displayed is an AFM picture of single $BaTiO_3$ nanoparticles immediately after ultrasonication and nanofiltering. The image shows that the nanoparticles have a diameter as well as a height in the range of 25–35 nm. Color code: dark corresponds to zero height and bright corresponds to 50 nm height. (*B*) Flatfield image calibration. Average corrected intensity over the whole spatial field of view versus different Dextran-Cascade blue concentrations. Three independent measurements for each concentration are shown. A linear regression fit to the first five data points is represented by a red line. (*C*) The normalized intensity distribution of the detected SHG diffraction-limited spots are shown in white columns. The red line represents the fitted sum of 2 Gaussians (black dash lines). The first peak indicates a single SHG nanocrystals, the second to aggregates.

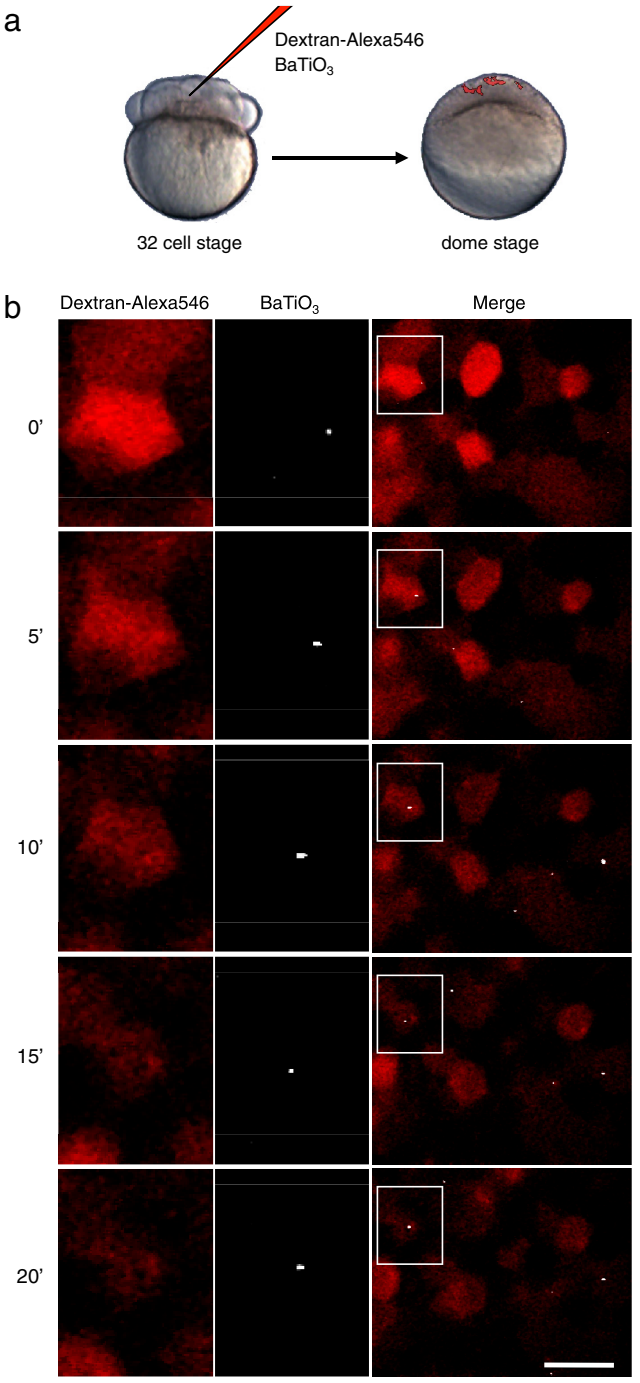

Fig. S3. SHG nanoprobes provide superior signal-to-noise ratio and do not bleach after in vivo injections. (*A*) Single-cell coinjections of $BaTiO_3$ nanoparticles and 10,000 MW Dextran-Alexa546 were performed at the 32-cell stage and imaged at the dome stage of zebrafish embryos. (*B*) Time-lapse images of individual cells at the dome stage of a zebrafish embryo marked with $BaTiO_3$ nanocrystals (*Center* column) and Dextran-Alexa546 (*Left* column). Right column is the merged picture with white boxes magnified in the center and left columns. Times (0′, 5′, 10′, 15′, and 20′) indicate minutes at and after the start of the experiment. Note that continuous scanning with intense excitation power levels bleaches quickly the organic dye, whereas the SHG signal of $BaTiO_3$ stays unchanged, allowing long-term nanoparticle tracking. Anterior to the left. Bar corresponds to 20 μm.

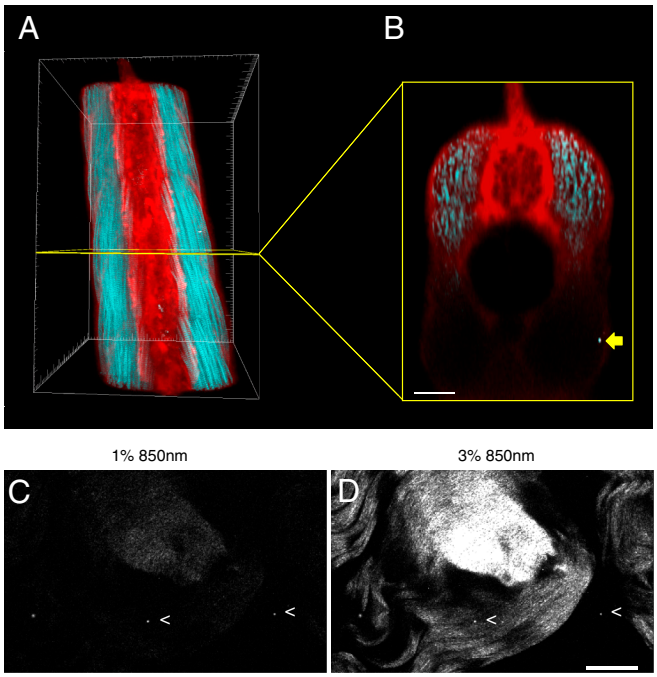

Fig. S4. SHG nanoprobes can be readily detected with increased imaging depth and provide superior signal-to-noise ratio when present in mammalian tail tendon. (*A* and *B*) $BaTiO_3$ nanocrystals were injected into one-cell stage colorless zebrafish embryos. Several days after cytoplasmic injection (around 72 hpf) part of the zebrafish trunk was imaged with femtosecond pulsed 820-nm light. (*A*) Dorsal 3D reconstruction of the zebrafish trunk showing endogenous SHG signal from trunk-muscles detected in transdirection (blue), SHG of $BaTiO_3$ nanocrystals detected in epi- as well as in transdetection (white), and BODIPY TR methyl ester dye labeling the extracellular matrix and cell membranes (red). Rostral front, caudal back. (*B*) Axial view of a slice of the trunk 3D reconstruction (yellow box). Whereas endogenous SHG and the vital dye are only readily detectable in the first 100 μm, the cross-sectional view through the trunk muscle shows that intense SHG signal of $BaTiO_3$ nanocrystals is still detectable with increased imaging depth [here, nanocrystals (yellow arrow) present in the trunk of a zebrafish at an imaging depth of around 200 μm]. Note that the power levels required to detect endogenous SHG are 10 times higher than those to visualize $BaTiO_3$. Bar corresponds to 50 μm. (*C* and *D*) $BaTiO_3$ nanocrystals present in mouse tail slices of approximately 2–3-mm thickness. (*C*) One percent excitation with femtosecond pulsed 850-nm light results in strong SHG signal from diffraction-limited $BaTiO_3$ nanocrystals (two of three spots marked with arrowheads) together with weak endogenous SHG signal originating from collagen in connective tissue of mouse tail tendon. (*D*) Increasing the excitation power level to 3% results in robust endogenous SHG signal with regular and highly organized collagen fiber clearly observable. Note that the power levels required to detect a strong signal from SHG nanocrystal signal spots is lower than for endogenous SHG of very highly aligned collagen fibers in mouse tail tendon. Bar corresponds to 50 μm.

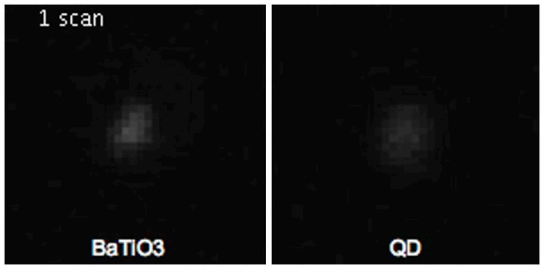

Movie S1. SHG nanoprobes neither bleach nor blink Time-lapse imaging of single $BaTiO_3$ nanocrystal (*Left*) and CdSe/ZnS quantum dot (*Right*) immobilized in 20% polyacrylamide gel and illuminated with low intensity levels of 820-nm light 300 times with a scanning speed of 20 frames/s.
Movie S1 (MOV)

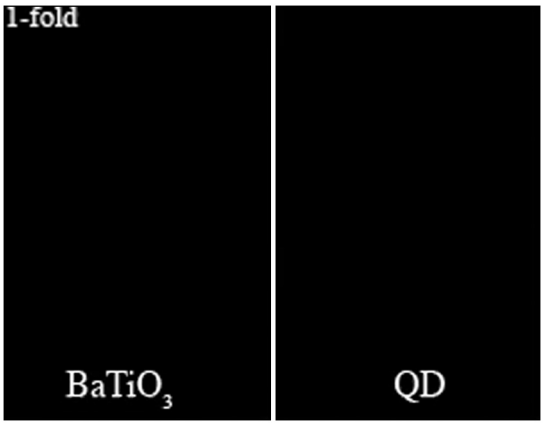

Movie S2. SHG nanoprobes do not saturate with increasing illumination intensity Image sequences of $BaTiO_3$ nanocrystal (*Left*) and CdSe/ZnS quantum dot (*Right*) immobilized in 20% polyacrylamide gel and rapidly illuminated with increasing 820-nm light intensity (1- to 40-fold).
Movie S2 (MOV)

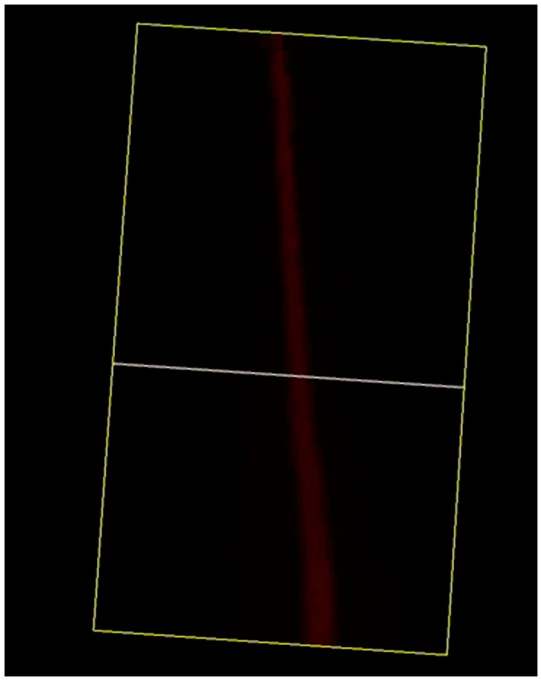

Movie S3. SHG nanoprobes can be readily detected with increased imaging depth 3D reconstruction of imaging z sections of the zebrafish trunk showing endogenous SHG signal from trunk muscles detected in transdirection (blue), SHG of $BaTiO_3$ nanocrystals detected in epi- as well as in transdetection (white and white), and BODIPY TR methyl ester dye labeling the extracellular matrix and cell membranes (red). In colorless mutant zebrafish embryos, light-scattering iridophores are significantly reduced.
Movie S3 (MOV)